ORIGINAL RESEARCH

Effect of mussel adhesive protein coating on osteogenesis in vitro and osteointegration in vivo to alkali-treated titanium with nanonetwork structures

Derong Yin[1]
Satoshi Komasa[1]
Shigeki Yoshimine[1]
Tohru Sekino[2]
Joji Okazaki[1]

[1]Department of Removable Prosthodontics and Occlusion, Osaka Dental University, Hirakata, Osaka, Japan; [2]Advanced Hard Materials, The Institute of Scientific and Industrial Research, Osaka University, Suita, Osaka, Japan

Purpose: On the basis of reasonable superposition of various surface treatment methods, alkali-treated titanium with nanonetwork structures (TNS) was coated with mussel adhesive protein (MAP) and named TNS-MAP. The aims were to optimize the biological properties of TNS, endue it with new properties, and enhance its utility in clinical dental applications.
Methods: TNS disks were coated with MAP and the product surface was characterized. Its osteogenic properties were determined by evaluating its effects on cell adhesion, cell proliferation, the expression of osteogenesis-related genes, and in vivo experiments.
Results: The treated materials showed excellent hydrophilicity, good surface roughness, and advantages of both TNS and MAP. TNS-MAP significantly promoted initial cell attachment especially after 15 mins and 30 mins. At every time point, cell adhesion and proliferation, the detection rate of osteogenesis-related markers in the extracellular matrix, and the expression of osteogenesis-related genes were markedly superior on TNS-MAP than the control. The in vivo experiments revealed that TNS-MAP promoted new bone growth around the implants and the bone–implant interface.
Conclusion: We verified through in vitro and in vivo experiments that we successfully created an effective TNS-MAP composite implant with excellent biocompatibility and advantages of both its TNS and MAP parent materials. Therefore, the new biocomposite implant material TNS-MAP may potentially serve in practical dentistry and orthopedics.
Keywords: biocomposite, bone marrow mesenchymal stem cell, extracellular matrix, nanopore, polydopamine

Introduction

Implant restoration is indispensable in prosthetic treatment and has gradually become increasingly familiar and acceptable to patients.[1,2] Consequently, the consumption of common biomedical materials such as titanium and titania has dramatically increased. Patient expectations of implant therapy efficacy have risen and may be important drivers in the ongoing investigation of implant materials.[3–5]

Recent studies on implant materials were not restricted to single-surface treatments. Researchers prefer to use at least two different implant treatments to improve biocompatibility. Certain investigators tried irradiating the surface of alkali-treated titanium with ultraviolet and applied other techniques to improve the antimicrobial and biocompatibility properties of the materials.[6–8] Others tested

Correspondence: Derong Yin
Department of Removable Prosthodontics and Occlusion, Osaka Dental University, 8-1 Kuzuha-hanazono-cho, Hirakata, Osaka 573-1121, Japan
Tel +81 72 864 3036
Fax +81 6 910 1044
Email y.d.r.nld@hotmail.com

cell sheets wrapped on the surfaces of titanium and zirconia implants. The novel MSC-Implant (bone marrow mesenchymal stem cell implant) may promote in vivo osteogenesis and vascularization and modify the implant surface.[9,10] These surface treatment methods may enhance the original biological properties of the basic materials and/or confer them with new biochemical properties.

Kim et al used alkali and heat treatments in the attempt to improve the biological properties of materials.[11] According to our previous study,[12–14] pure titanium implants formed a titanate layer with nanonetwork structures (TNS) after treatment with 10 M NaOH at 30°C. This modification made the implants more efficacious than untreated pure titanium both in vitro and in vivo because it promoted cell adhesion, proliferation, and osteogenesis-related gene expression. N-acetyl cysteine was applied to the surface of TNS material containing nanosilver cations to improve its antimicrobial property. The treatment also enhanced its ability to inhibit intracellular ROS.[7]

Mussels are marine bivalves firmly adhering to rocks under strong wave action.[15,16] They secrete mussel adhesive protein (MAP) from their byssal threads and adhesive plaques.[17,18] MAP is biocompatible, biodegradable, and nontoxic.[18–24] Mussels produce the proteins Mefp-1 in the byssus, Mefp-2 in the adhesive panel, and others.[18,25] All proteins with adhesive properties have the posttranslationally modified amino acid 3,4-dihydroxyphenyl-L-alanine (DOPA) and had high isoelectric points. The properties of MAP have inspired the development of biomaterials retaining their adhesiveness in liquid environments.[26,27] Researchers have attempted to use dopamine as a new surface treatment. When it is oxidized and self-polymerized under specific conditions, dopamine forms a polymer layer on almost any surface.[28] It is highly biocompatible and biodegradable and does not trigger immune responses.[18–24] Thus, MAP is regarded as a valuable biological material. Over the past 20 years, scholars have analyzed the basic structures, adhesion mechanisms, and cell and tissue effects of natural MAP extracts or their synthetic derivatives.[19,29–34] Recent studies showed that MAP increases cell adsorption on the surface of the base material.[28,35] Biocoated materials were created by directly coating the surfaces of three-dimensional scaffolds with MAP. In vivo experiments on a rat calvaria defect model showed that MAP substantially promotes bone regeneration.[36] We hypothesize, then, that a combination of MAP and TNS could increase the adhesiveness of TNS materials.

In the present study, we coated the surfaces of TNS materials with MAP and used in vitro and in vivo experiments to determine whether the resultant composites (TNS-MAP) were biologically superior to TNS alone. We also provided an experimental basis for further research into the potential clinical applications of this novel material.

Materials and methods
Sample preparation
Pure titanium disks (diameter 15 mm; thickness 1 mm) were prepared by machine (Engineering Test Service, Osaka, Japan) and sequentially polished with several grades of abrasive paper (Waterproof Paper® Nos. 800, 1,000, and 1,500; Riken Corundum Co. Ltd., Saitama, Japan). Pure titanium screw implants (external diameter 1.2 mm; length 12 mm) were also machined (Nishimura Metal, Fukui, Japan) and used in surface characterization and the in vitro and in vivo studies. The disks and screw implants were ultrasonically cleaned with acetone, ethanol, and deionized water in succession for 10 mins per step. They were dried overnight at room temperature (20–25°C). The materials were immersed in 10 M NaOH at 30°C for 24 hrs and rinsed ≥3× with ultrapure water until rinsate conductivity was <5 μS/cm^3. The dried final product was TNS. All TNS materials were sterilized by dry heat. Half of them were coated with MAP on a clean bench using the protein product concentration recommended by the manufacturer (Corning® Cell-Tak™). The product, named TNS-MAP, was cleaned with sterile deionized water and dried on a clean bench.

Surface analysis
TNS and TNS-MAP surface morphologies were examined by scanning electron microscopy (SEM) (S-4800; Hitachi, Tokyo, Japan). Surface topography and mean average surface roughness (Ra) were examined by atomic force microscopy (AFM) (SPM-9600; Shimadzu, Tokyo, Japan). The chemical compositions of the modified surface layers were analyzed by X-ray photoelectron spectrometry (XPS; PHI X-tool; ULVAC-PHI, Kanagawa, Japan). Contact angles were measured with a contact angle measurement system (VSA 2500 XE; AST Products, Billerica, MA, USA). The physicochemical properties of TNS and TNS-MAP were determined by attenuated reflectance Fourier transform infrared spectroscopy (ATR-FTIR)

over a range of 400–4,000 cm^{-1} with a Spectrum One instrument (PerkinElmer, Norwalk, CT, USA).

Cell culture

Rat bone marrow mesenchymal stem cells (rBMMSCs) were extracted from the femurs of 8-week Sprague–Dawley rats (Shimizu Laboratory Supplies Co., Kyoto, Japan) and incubated in 75-cm^2 flasks according to a previously described method.[6] The third- and fourth-cell generations were used in in vitro experiments. They were digested with trypsin, resuspended, and added to 24-well plates containing TNS and TNS-MAP disks at a density of 4×10^4 cells/well. This study was performed in accordance with the Guidelines for Animal Experimentation at Osaka Dental University (Approval No. 18-03007).

Cell adhesion and proliferation

Cell adhesion and proliferation were assessed by CellTiter-Blue® Cell Viability Assay (Promega, Madison, WI, USA) according to the manufacturer's protocol. The time points for cell adhesion measurement were 15 mins, 30 mins, 1 hr, and 3 hrs. Cell proliferation was evaluated at 1 day, 3 days, and 7 days. Incubated samples were washed twice with PBS and treated with 300 µL diluted Cell Titer-Blue® Reagent consisting of 50 µL Cell Titer-Blue® Reagent diluted in 250 µL PBS and prepared immediately before the PBS wash. After 1 hr incubation (37°C; 5% CO$_2$), 100 µL reagent from each well was added to a 96-well tissue culture plate and fluorescence was measured at 560/590 nm in a microplate reader (SpectraMax M5; Molecular Devices, San Jose, CA, USA).

Cell morphology

After 6-hr incubation, the media in all 24-well plates were removed. The cells were washed 3× with PBS and mixed with 1 mL of 4% PFA (paraformaldehyde solution) per well. After 20 mins, the cells were washed 3× with PBS and permeabilized with 0.2% (v/v) Triton X-100 for 30 mins at room temperature (20–25°C) with shaking for 30 s. After 30 mins, the cells were incubated with Blocking One reagent (Nacalai Tesque Inc., Kyoto, Japan) for 30 mins at room temperature (20–25°C) and stained with phalloidin and DAPI at 37°C in the dark for 1 hr. The stained cells were washed 3× with PBS and F-actin, and nuclei in the cells were examined under a confocal laser-scanning microscope (LSM700; Carl Zeiss AG, Wetzlar, Germany).

ALP activity

After 1-week cell culture, the medium was replaced with differentiation-inducing medium containing 10% FBS, antibiotic–antimycotic mix, and the osteogenic supplements 10 mM β-glycerophosphate (Wako Pure Chemical Industries Ltd., Osaka, Japan), ascorbic acid (Nacalai Tesque Inc.), and 10 nM dexamethasone (Nacalai Tesque Inc.). The medium was exchanged, and the cells were incubated for 7 days and 14 days. The samples were washed with PBS and lysed with 300 µL of 0.2% Triton X-100. The lysates were transferred to microcentrifuge tubes, and the ALP activity was measured using ALP pNPP Liquid substrate in an ELISA kit (Sigma-Aldrich Corp., St Louis, MO, USA) according to the manufacturer's protocol. The reaction was terminated by adding 50 µL of 3 M NaOH to 200 µL of the reaction substrate. The p-nitrophenol production was determined at 405 nm in a 96-well microplate reader (SpectraMax® M5; Molecular Devices). The DNA content was determined with a PicoGreen dsDNA Assay Kit (Thermo Fisher Scientific, Waltham, MA, USA), according to the manufacturer's protocol. The amount of ALP was normalized to that of the DNA content of the respective cell lysates.

Quantification of calcium deposition in the extracellular matrix (ECM)

The medium was replaced and incubation continued for 21 days and 28 days. Calcium deposited in the ECM was dissolved with 10% formic acid, collected, and quantified with a calcium E-test kit (Wako Pure Chemical Industries Ltd.) per a previous study.[37]

Analysis of osteogenesis-related gene expression levels

The total RNA of rBMMSCs cultured for 3 days, 7 days, 14 days, and 21 days on sample TNS and TNS-MAP disks was isolated with the RNeasy Mini Kit (Qiagen, Venlo, The Netherlands) and a TaqMan real-time RT-PCR assay (Life Technologies, Carlsbad, CA, USA), as previously described.[6] A PrimeScript RT Reagent Kit (TaKaRa Bio, Kusatsu, Shiga, Japan) was used to reverse-transcribe 10-µL aliquots of each RNA sample into cDNA. *ALP* and runt-related transcription factor 2 (*Runx2*) expression levels were measured at 3 days and 7 days. The expression levels of bone morphogenetic protein 2 (*BMP-2*) and bone γ-carboxyglutamate (gla) protein (*Bglap*) were measured at 14 days and 21 days. The StepOne™ Plus RT-PCR

System (Life Technologies) was used to quantify these osteogenesis-related genes. The relative gene expression levels of each group were normalized to that of the housekeeping gene glyceraldehyde 3-phosphate dehydrogenase (*GAPDH*) and determined by the $2^{-\Delta\Delta Ct}$ method.[12]

Animal model and surgical procedures

Ten male Sprague–Dawley rats aged 8 weeks (Shimizu Laboratory Supplies Co.) were randomly assigned to each of two groups. The experimental method used was described in a previous report.[38] The operation was performed aseptically, and the animal study was conducted in accordance with the ethical guidelines of the Animal Care and Use Committee of Osaka Dental University (Approval No. 18-03007).

Microcomputed tomography (micro-CT) assessment

Right femurs with implants were excised per a previously described method and scanned with the SMX-130CT micro-CT scanner (Shimadzu Corp.) at 70 kV and 118 mA.[38] Morphometric software (TRI/3D-BON; Ratoc System Engineering, Tokyo, Japan) was used to analyze the regions of interest (ROI; 500 μm around the implant and 2 mm below the epiphyseal line) in the CT images and evaluate the bone volume fraction (BV/TV, %), trabecular

number (Tb.N, mm^{-1}), trabecular separation (Tb.Sp, μm), and trabecular thickness (Tb.Th, μm).

Histological section preparation and analysis

Rat femur specimens (8 weeks) were scanned by micro-CT, excised, and stained by the Villanueva method to assess osseointegration and bone regeneration (bone area ratio, BA; bone–implant contact, BIC) under a BZ-9000 digital cold illumination microscope (Keyence Co., Osaka, Japan).[39]

Statistical analysis

Surface analyses and in vitro and in vivo experiments were conducted in triplicate. All data are reported as means ± SD. Differences between treatment means were evaluated by one-way ANOVA and Student's *t*-test in SPSS v. 20.0 (IBM Corp., Armonk, NY, USA). Differences were considered statistically significant at $P<0.05$.

Results
Surface characterization

SEM and AFM revealed the surface morphology of TNS and TNS-MAP. Figure 1A and B show the nanoporous network structure on the TNS surface at 10.0 k and 45.0 k, respectively. Figure 1D shows MAP thoroughly coating the TNS surface
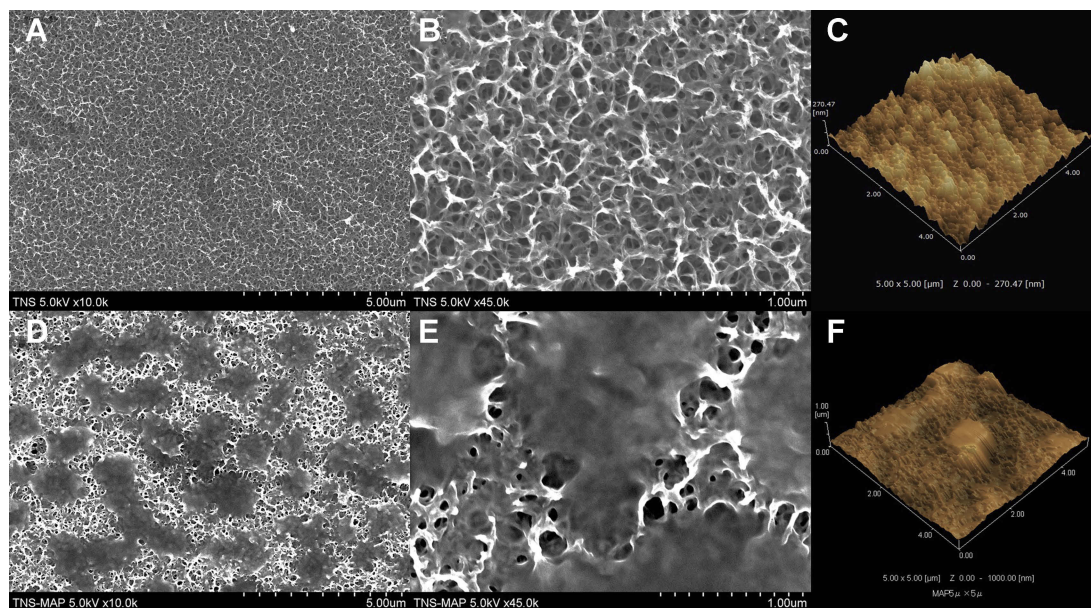
Figure 1 SEM micrographs and AFM images of TNS and TNS-MAP.
Notes: (**A**–**C**) TNS surface, and (**D**–**F**) TNS-MAP surface.
Abbreviations: SEM, scanning electron microscopy; AFM, atomic force microscopy; TNS, titanium with nanonetwork structures; TNS-MAP, titanium with nanonetwork structures coated with mussel adhesive protein.

and the nanoporous network structure. Figure 1E shows the same at a higher magnification (45.0 k).

The AFM images show the nanotopography of the TNS and TNS-MAP surfaces. Figure 1C is the AFM image of the uniform nanoporous network structure of the TNS surface. The MAP protrusions on the TNS surface are shown in Figure 1F. The surface roughness (Ra) values measured by AFM were 74.627 for MAP and 30.910 for TNS (nanoscale).

Contact angle measurements (Figure 2) demonstrated that both TNS and TNS-MAP were more hydrophilic and diffused ddH_2O more effectively than pure Ti. The hydrophilicity of TNS-MAP is significantly higher than that of TNS ($P<0.05$).

The XPS analysis of the materials (Figure 3) disclosed that, relative to TNS, the percentages of Ti2p and O1s were lower on the TNS-MAP surface. The proportion of N1s (a protein component) in TNS-MAP was 13%, whereas it was 0% in TNS. The proportion of C1s in TNS-MAP was greater than that of TNS.

The FTIR spectra of the test and control groups are presented in Figure 4. For the TNS-MAP group, the sensor surface showed bands at $\sim 1,500$ cm^{-1} and $\sim 1,750$ cm^{-1} compared with the TNS group. Baty et al reported similar FTIR spectral data for the MAP.[40] The surface morphology and chemical analyses confirmed that the MAP successfully coated the TNS surface.

Cell adhesion, proliferation, and morphology

The adhesion of rBMMSCs on the TNS-MAP surface was superior to that for TNS at various time points, especially at 15 mins and 30 mins (Figure 5A). At 1 day, 3 days, and 7 days, there was more cell proliferation on the TNS-MAP than the TNS surface (Figure 5B).

Fluorescent staining revealed that after 6-hr cell culture (Figure 5C and D), the number of cells adhering to the TNS-MAP surface was greater than that for TNS.
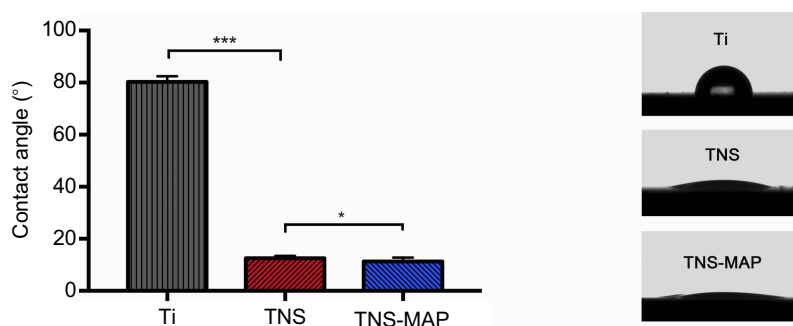
**Figure 2** Comparison of contact angle measurements for pure Ti, TNS, and TNS-MAP.
Notes: Contact angles of Ti, TNS, and TNS-MAP were measured with a VSA2500 XE contact angle measurement system after application of 2 µL ddH_2O to the sample surface at room temperature (***$P<0.001$; *$P<0.05$).
Abbreviations: Ti, titanium; TNS, titanium with nanonetwork structures; TNS-MAP, titanium with nanonetwork structures coated with mussel adhesive protein.
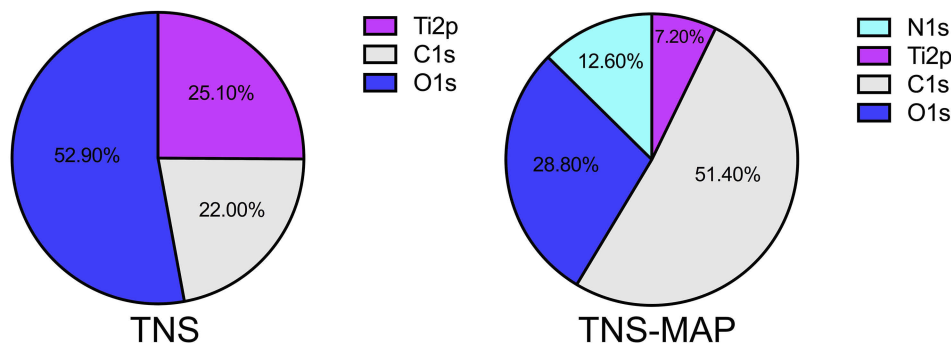
**Figure 3** Surface chemical compositions of specimens examined by XPS.
Abbreviations: XPS, X-ray photoelectron spectroscopy; TNS, titanium with nanonetwork structures; TNS-MAP, titanium with nanonetwork structures coated with mussel adhesive protein.
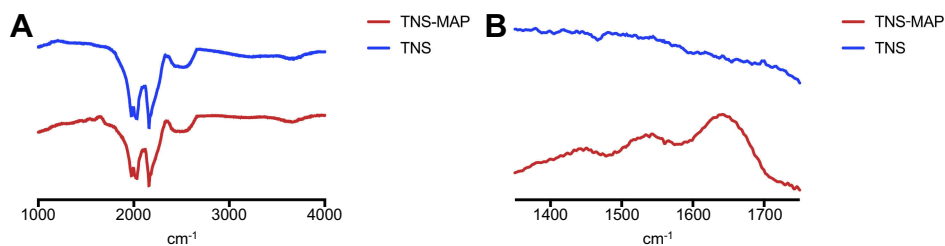
Figure 4 FTIR analysis of TNS and TNS-MAP.
Notes:(**A**) cm^{-1} from 1,000 to 4,000, and (**B**) cm^{-1} from 1,350 to 1,750.
Abbreviations: FTIR, Fourier transform infrared spectroscopy; TNS, titanium with nanonetwork structures; TNS-MAP, titanium with nanonetwork structures coated with mussel adhesive protein.
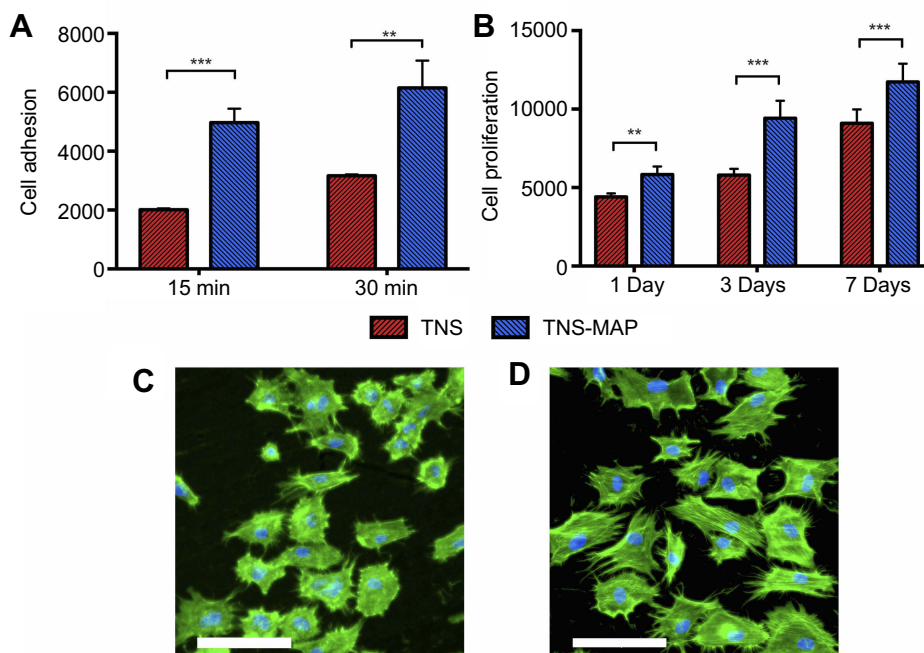
Figure 5 Cell adhesion, proliferation, and morphological analysis of rBMMSCs on sample disks.
Notes: (**A** and **B**) TNS and TNS-MAP disks were incubated with rBMMSCs and cell adhesion and proliferation were evaluated after 15 mins, 30 mins, 1 day, 3 days and 7days, respectively, with a CellTiter-Blue® Cell Viability Assay (Promega, Madison, WI, USA), (**C** and **D**) TNS and TNS-MAP disks were incubated with rBMMSCs for 6 hrs, stained with phalloidin (F-actin) and DAPI (nuclei), and visualized by fluorescence microscopy; bar =100 μm. (***P<0.001; **P<0.01).
Abbreviations: rBMMSCs, rat bone marrow mesenchymal stem cells; TNS, titanium with nanonetwork structures; TNS-MAP, titanium with nanonetwork structures coated with mussel adhesive protein.

Moreover, the cells spread more uniformly over the TNS-MAP surface than the TNS surface.

Osteogenic activity of rBMMSCs

After 7-day and 14-day induction of cell differentiation on the surfaces of the materials, the cells on TNS-MAP had higher ALP activity than those on TNS (Figure 6).

Calcium was measured in the ECM after inducing mineralization for 21 days and 28 days. The cells on TNS-MAP secreted more Ca than those on TNS (Figure 6).

The osteogenic differentiation-related genes *Runx2* and *ALP* were upregulated on TNS-MAP compared to TNS in the early stages (3 days and 7 days; Figure 7A and B). Similarly, *Bglap* and *BMP-2* were more highly expressed on TNS-MAP than TNS after 14-day and 21-day culture (Figure 7C and D).

Micro-CT assessment

The surgical procedure is shown in Figure 8. In the ROI, TNS-MAP formed more new bone around the implant than TNS.
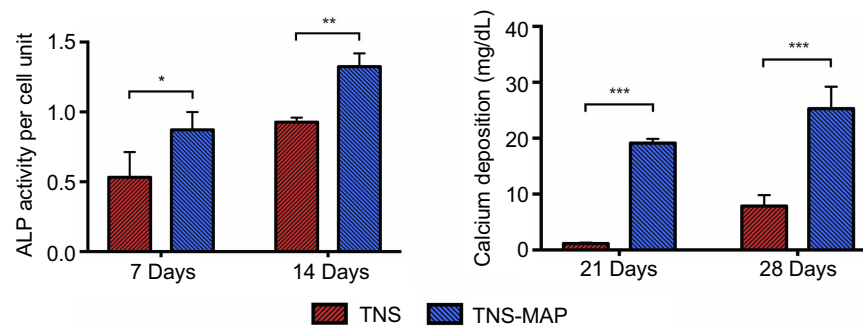
Figure 6 ALP activity and calcium deposition in cells grown on sample disks.
Notes: rBMMSCs were cultivated on TNS and TNS-MAP disks for up to 28 days and the levels of (**A**) ALP activity (7 days and 14 days) and (**B**) calcium deposition (21 days and 28 days) were evaluated as described in the "Materials and Methods" (***$P<0.001$; **$P<0.01$; *$P<0.05$).
Abbreviations: ALP, alkaline phosphatase; rBMMSCs, rat bone marrow mesenchymal stem cells; TNS, titanium with nanonetwork structures; TNS-MAP, titanium with nanonetwork structures coated with mussel adhesive protein.
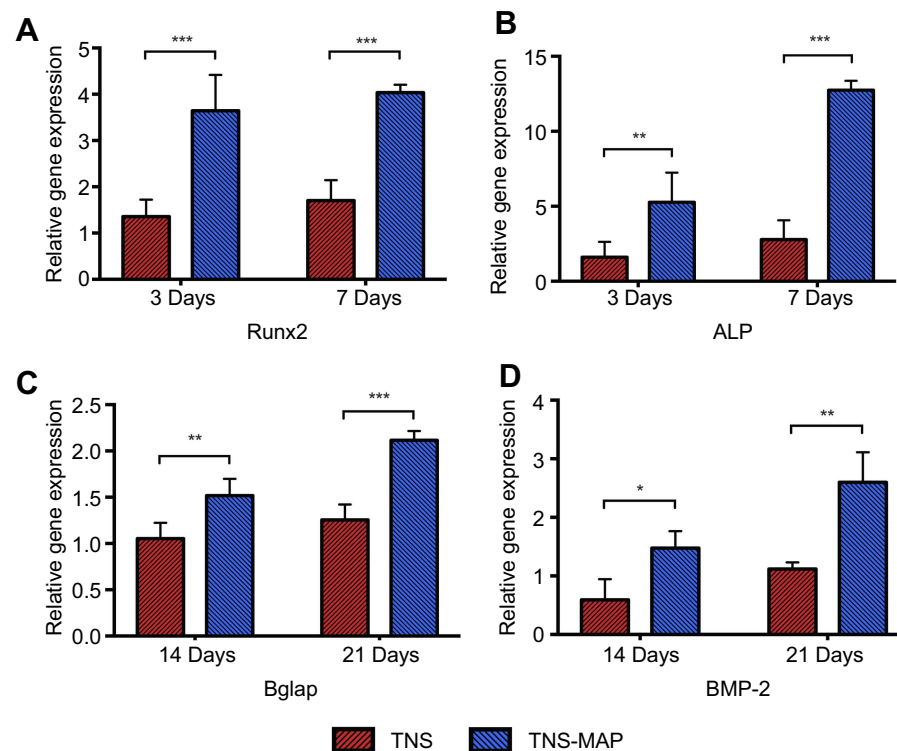
**Figure 7** Expression of osteogenesis-related genes in cells grown on sample disks.
Notes: (**A–D**): Expression levels of genes encoding *Runx2*, *ALP*, *Bglap*, and *BMP-2* were evaluated in rBMMSCs cultivated on TNS and TNS-MAP disks at days 3 and 7 and days 14 and 21, respectively, by real-time RT-PCR (***$P<0.001$; **$P<0.01$; *$P<0.05$).
Abbreviations: *Runx2*, runt-related transcription factor 2; *ALP*, alkaline phosphatase; *Bglap*, bone γ-carboxyglutamate (gla) protein; *BMP-2*, bone morphogenetic protein 2; rBMMSCs, rat bone marrow mesenchymal stem cells; TNS, titanium with nanonetwork structures; TNS-MAP, titanium with nanonetwork structures coated with mussel adhesive protein.

Three-dimensional images are shown in Figure 9A and B (implant in red, cortical bone in blue, and new bone in kelly green). As shown in Figure 10, quantitative assessment of trabecular bone in the ROI disclosed that BV/TV, Tb.N, and Tb.Th for TNS-MAP were significantly higher than those for TNS. However, Tb.Sp was lower for TNS-MAP than TNS.

Histological evaluation

Longitudinal images of the implant and surrounding bone tissue are presented in Figure 11A and B. The amount of new bone attached to the surface of the TNS-MAP implant was greater than that of the TNS implant. At 8 weeks after surgery, both the BA and the BIC of the TNS-MAP
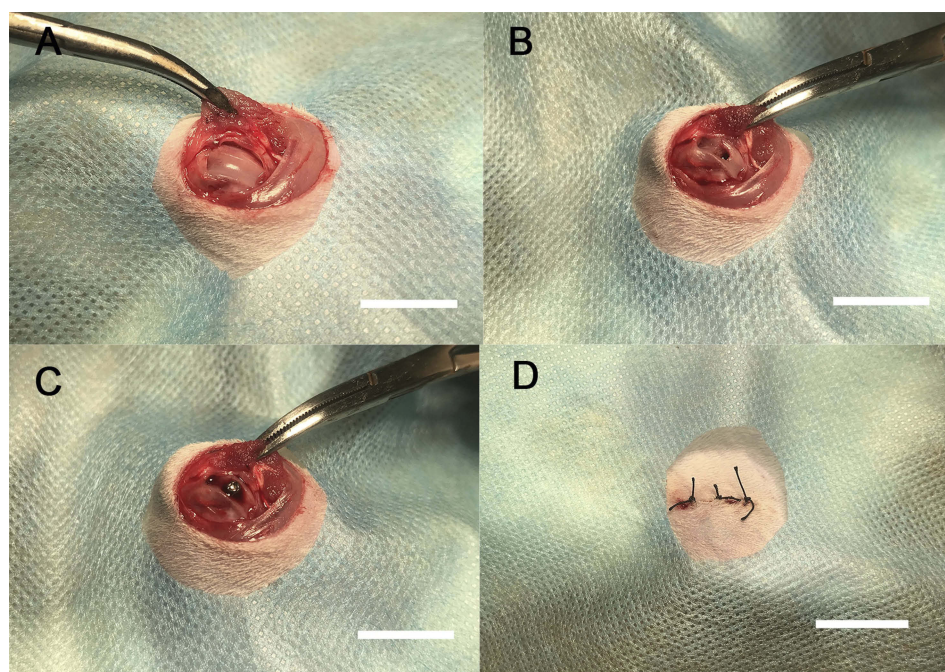
Figure 8 In vivo experimental operation.
Notes: (**A**) Incision and exposure of surgical area, (**B**) implantation model formation, (**C**) implant embedment, and (**D**) suture of surgical area; bar =1 cm.
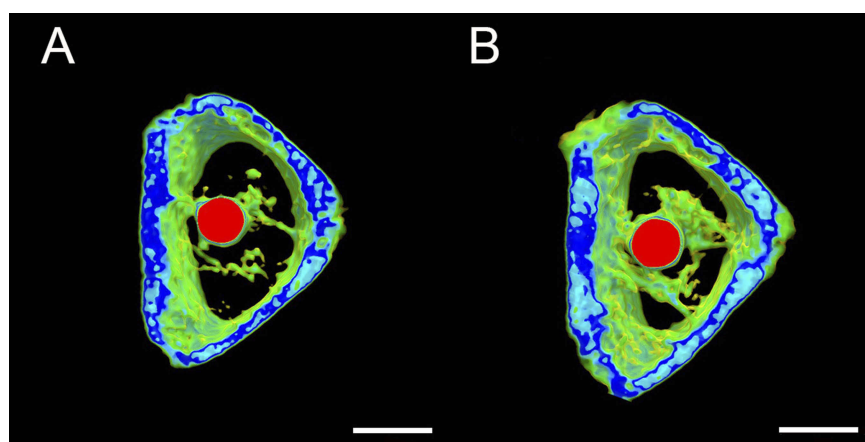
Figure 9 Transverse micro-CT reconstructed images of proximal tibiae showing ROI status.
Notes: Implant (red), newly formed bone with relatively low density (kelly green), and cortical bone with high density (blue). (**A**) 8-week TNS group, and (**B**) 8-week TNS-MAP group; bar =2 mm.
Abbreviations: micro-CT, micro-computed tomography; TNS, titanium with nanonetwork structures; TNS-MAP, titanium with nanonetwork structures coated with mussel adhesive protein; ROI, region of interest.

implants were significantly higher than those of the TNS implants (Figure 12; $P<0.05$).

Discussion

In the present study, the surface characteristics of TNS and TNS-MAP were investigated and cell adhesion, cell proliferation, and osteogenic differentiation-related gene expression were analyzed. In vivo experiments were conducted using both TNS and TNS-MAP. The results showed that MAP successfully coated the TNS surface and TNS-MAP was more efficacious at early adhesion, proliferation, and osteogenic rBMMSC differentiation than TNS. The findings of the in vivo experiment corroborated those of the in vitro experiment.

SEM and AFM disclosed that a nanoporous network structure was formed on the TNS surface after alkali treatment at room temperature possibly because of hydrogen formation during the treatment process. Moreover, the
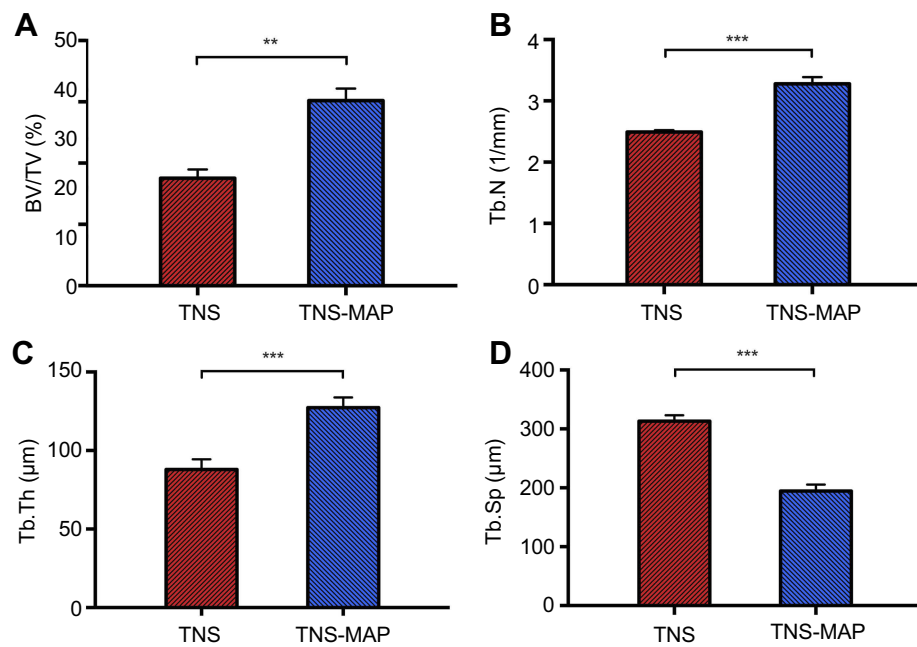
**Figure 10** Micro-CT quantitative evaluation within the ROI.
Notes: (**A**) Bone volume fraction of the two groups, (**B**) Tb.N of the two groups, (**C**) Tb.Th of the two groups, and (**D**) Tb.Sp of the two groups (***$P<0.001$; **$P<0.01$).
Abbreviations: micro-CT, micro-computed tomography; ROI, region of interest; BV/TV, bone volume/total volume; Tb.N, trabecular number; Tb.Th, trabecular thickness; Tb.Sp, trabecular separation; TNS, titanium with nanonetwork structures; TNS-MAP, titanium with nanonetwork structures coated with mussel adhesive protein.
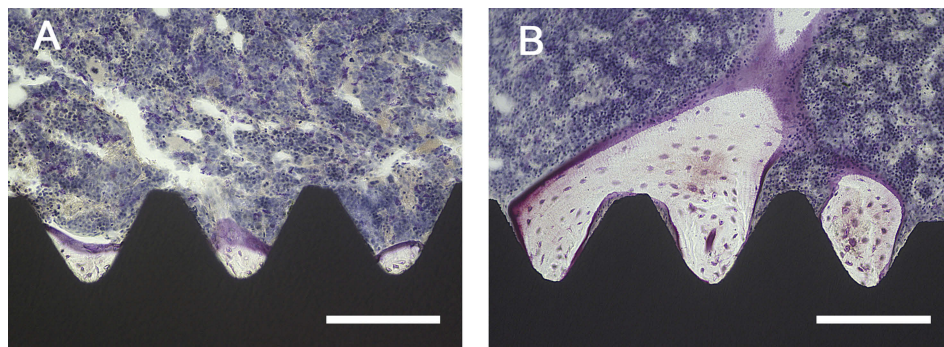
Figure 11 Histological sections with Villanueva staining showing bone tissue morphology around the implant (black).
Notes: (**A**) TNS surface, and (**B**) TNS-MAP surface; bar =200 µm (***$P<0.001$; **$P<0.01$).
Abbreviations: TNS, titanium with nanonetwork structures; TNS-MAP, titanium with nanonetwork structures coated with mussel adhesive protein.
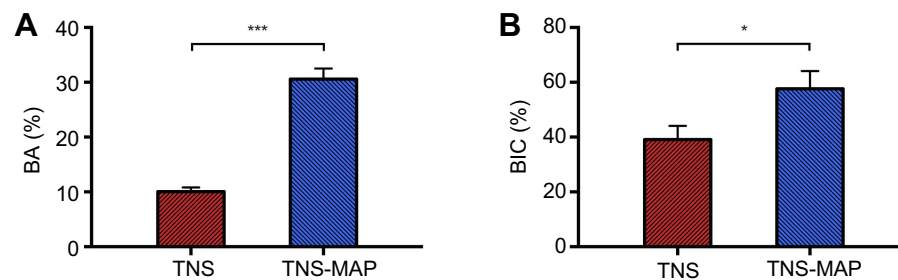
Figure 12 Quantitative histomorphometric analysis within the region of measurement (BA and BIC).
Notes: (**A**) Percentage of new bone formation (BA) and (**B**) percentage of direct BIC (***$P<0.001$; *$P<0.05$).
Abbreviations: BA, bone area ratio; BIC, bone–implant contact; TNS, titanium with nanonetwork structures; TNS-MAP, titanium with nanonetwork structures coated with mussel adhesive protein.

NaOH treatment may have broken the Ti–O–Ti bonds and generated Ti–O–Na and Ti–OH layers on the titanium surface.[13,41] MAP thoroughly coated the TNS surface and FTIR and XPS revealed that it formed TNS-MAP.

MAP permeated the nanoporous network structure of TNS. The result of AFM revealed that the Ra of TNS and TNS-MAP were both within 100 nm, therefore, both of TNS and TNS-MAP are nanoscale materials.[12] The Ra of TNS-MAP was greater than that of TNS and had relatively higher surface roughness. In TNS, there was no interface between the nanostructure and pure basal titanium. MAP firmly adhered to the TNS nanostructure[28,42] rather than simply coating it. XPS analysis of TNS-MAP indicated that the Ti2p element on the TNS-MAP was either ~0 or >0 and nearly equal to the amount on TNS. The combined SEM and AFM images showed that MAP successfully coated the TNS. The interval between the MAP layers effectively retained part of the nanoporous network structure. Therefore, the composite material has characteristics of both TNS and MAP. The contact angle measurement showed that the alkali treatment and the MAP coating optimized the surface hydrophilicities of pure Ti and TNS material, respectively, and the differences were significant. Increases in surface material hydrophilicity promote cell adhesion.[28]

Cell adhesion, proliferation, and osteogenic activity were also analyzed. Adhesion plays important roles in cell spreading and differentiation, tissue engineering, and other processes.[28] After 6-hr seeding, cell staining revealed that the surface adhesion of TNS-MAP was superior to that of TNS and spreading markedly increased. A previous study showed that MAP promoted early cell adhesion but not cell spreading.[18] As the composite material has advantages of both MAP and TNS, it may promote cell spreading and improve cell adhesion.

Early cell adhesion indicated that TNS-MAP significantly enhanced cell adhesion on TNS at 15 mins ($P<0.001$) and 30 mins ($P<0.01$) after seeding. No such observation was reported for an earlier study on TNS. The MAP coating optimized the biological performance of TNS. The MAP used in the present study was a mixture of Mefp-1 and Mefp-2 extracted from mussels.[18] The mechanism of cell adhesion on the DOPA coating material surface was described elsewhere.[28,43] The surfaces of materials coated with polydopamine may adhere specifically or nonspecifically.[28,43] In nonspecific cell adhesion, chemical functional groups on the biomaterial surface may bind weakly to cell membranes through van der Waals forces or electrostatic interactions. In specific cell adhesion,

polydopamine forms very thin cell adhesion protein domains on the biomaterial surfaces and binds the cells.[43] The presence and concentration of DOPA[18,25] in Mefp-1 and Mefp-2 partially explain why TNS-MAP induces cell adhesion. TNS-MAP promoted cell adhesion and proliferation more effectively than TNS at every time point. ECM-derived adhesion proteins and growth factors can efficiently attach to surfaces modified with DOPA.[44,45] Studies have suggested that rMSC may be induced by nanotopographical signals through FA and actomyosin cytoskeleton contractility.[46] The nanostructure and superior hydrophilicity of the surface material also induce cell adhesion.[12,13,47–49]

ALP activity and calcium precipitation in the ECM indicated that TNS-MAP induces osteogenic differentiation more effectively than TNS alone. The relatively greater mRNA upregulation in the former at every time point corroborated this observation. The expression levels of four genes involved in bone marrow stem cell differentiation and osteogenesis, and their importance in these processes was reported elsewhere.[12,50,51]

Micro-CT and histological analyses revealed that new bone formation around the TNS-MAP implant was substantially greater than that around TNS. The relative improvement of BIC in the former case also demonstrates that the TNS-MAP implant undergoes more efficacious early osseointegration with the recipient area than the TNS implant.

Biomaterials functionalized with various molecules induce specific reactions in cells or tissues.[28] The appropriate material surface enhances cellular extension morphology and promotes cell proliferation and differentiation ability there. Certain authors focused on DOPA as an intermediate carrier of growth factors such as BMP-2, BMP-7, and others in the surface treatment of various biomaterials. In this way, it promotes osteogenic differentiation in BMMSCs both in vitro and in vivo. This molecular mechanism has already been explained.[52–54] BMP-2 promotes fracture healing and shortens integration time. As they are highly adhesive, TNS-MAP implants may adsorb BMP-2 and other growth factors in the bone marrow cavity. In this manner, they promote osteogenic differentiation in the BMMSCs attached to their surfaces. Studies have shown that a DOPA coating promotes osteogenic differentiation via a focal adhesion kinase (FAK) cascade.[55] The expression of FAK is an important factor in FA activation.[56] FA formation initiates interactions between the cells and the substrate. In addition, rMBCs can be induced by nanostructures via FA, etc.[57] Previous

researchers evaluated integrin β1, integrin β3, and FAK expression and established that DOPA-treated materials promoted rMSC adhesion and spreading.[45] These processes may partially account for the mechanisms by which TNS-MAP promotes rBMMSCs adhesion, proliferation, and osteogenic differentiation. However, the exact and detailed molecular mechanisms are still unclear and merit further investigation.

Detailed analyses of the material surfaces verified that the TNS-MAP composite implant was successfully created. It has advantages of both TNS and MAP, is highly biocompatible, and has good surface roughness and excellent hydrophilicity. Its physicochemical properties promote early cell adhesion and enable attached cells to proliferate and differentiate. In future research, the immunological and other characteristics of TNS-MAP will be explored and its clinical chemistry and applications will be investigated.

Conclusion

Surface analyses and cell experiments involving TNS and TNS-MAP showed that the latter MAP had superior hydrophilicity and rBMMSC cell biocompatibility to TNS because of its MAP coating. TNS-MAP may more effectively promote early cell adhesion and proliferation and induce osteogenic cell differentiation. The in vivo experiment indicated that TNS-MAP improved BA and BIC compared to TNS and confirmed that TNS-MAP is more biocompatible than TNS. Thus, TNS-MAP has great potential applicability in dentistry and orthopedics.

Acknowledgments

Disclosure

The authors report no conflicts of interest in this work.

References

1. Kashbour WA, Rousseau NS, Thomason JM, Ellis JS. Provision of information on dental implant treatment: patients' thoughts and experiences. *Clin Oral Implants Res*. 2018;29(3):309–319.
2. Exley CE, Rousseau NS, Steele J, et al. Paying for treatments? Influences on negotiating clinical need and decision-making for dental implant treatment. *BMC Health Serv Res*. 2009;9:7.
3. Yao J, Tang H, Gao X-L, McGrath C, Mattheos N. Patients' expectations from dental implants: A systematic review of the literature. *Health Qual Life Outcomes*. 2014;12:153.
4. Yao J, Li M, Tang H, et al. What do patients expect from treatment with Dental Implants? Perceptions, expectations and misconceptions: a multicenter study. *Clin Oral Implants Res*. 2017;28(3):261–271.
5. Abrahamsson KH, Wennström JL, Berglundh T, Abrahamsson I. Altered expectations on dental implant therapy; views of patients referred for treatment of peri-implantitis. *Clin Oral Implants Res*. 2017;28(4):437–442.
6. Zhang H, Komasa S, Mashimo C, Sekino T, Okazaki J. Effect of ultraviolet treatment on bacterial attachment and osteogenic activity to alkali-treated titanium with nanonetwork structures. *Int J Nanomed*. 2017;12:4633–4646.
7. Zhang H, Hatoko M, Yin D, et al. Antibacterial activity and biocompatibility of nanoporous titanium doped with silver nanoparticles and coated with n-acetyl cysteine. *J Hard Tissue Biol*. 2018;27(4):351–358.
8. Wang G, Feng H, Hu L, et al. An antibacterial platform based on capacitive carbon-doped TiO 2 nanotubes after direct or alternating current charging. *Nat Commun*. 2018;9(1):2055.
9. Zhou W, Han C, Song Y, et al. The performance of bone marrow mesenchymal stem cell - Implant complexes prepared by cell sheet engineering techniques. *Biomaterials*. 2010;31(12):3212–3221.
10. Yu M, Zhou W, Song Y, et al. Development of mesenchymal stem cell-implant complexes by cultured cells sheet enhances osseointegration in type 2 diabetic rat model. *Bone*. 2011;49(3):387–394.
11. Kim HM, Miyaji F, Kokubo T, Nakamura T. Preparation of bioactive Ti and its alloys via simple chemical surface treatment. *J Biomed Mater Res*. 1996;32(3):409–417.
12. Xing H, Komasa S, Taguchi Y, Sekino T, Okazaki J. Osteogenic activity of titanium surfaces with nanonetwork structures. *Int J Nanomed*. 2014;9(1):1741–1755.
13. Komasa S, Taguchi Y, Nishida H, Tanaka M, Kawazoe T. Bioactivity of nanostructure on titanium surface modified by chemical processing at room temperature. *J Prosthodont Res*. 2012;56(3):170–177.
14. Kusumoto T, Yin D, Zhang H, et al. Evaluation of the osteointegration of a novel alkali-treated implant system in vivo. *J Hard Tissue Biol*. 2017;26(4):355–360.
15. Waite JH. Evidence for a repeating 3,4-dihydroxyphenylalanine- and hydroxyproline-containing decapeptide in the adhesive protein of the mussel, *Mytilus edulis* L. *J Biol Chem*. 1983;258(5):2911–2915.
16. Kamino K, Inoue K, Maruyama T, Takamatsu N, Harayama S, Shizuri Y. Barnacle cement proteins: importance of disulfide bonds in their insolubility. *J Biol Chem*. 2000;275(35):27360–27365.
17. Waite JH. Polyphenolic substance of *Mytilus edulis*: novel. *Science*. 1981;212(29):1038–1040.
18. Cha HJ, Hwang DS, Lim S. Development of bioadhesives from marine mussels. *Biotechnol J*. 2008;3(5):631–638.
19. Hwang DS, Gim Y, Yoo HJ, Cha HJ. Practical recombinant hybrid mussel bioadhesive fp-151. *Biomaterials*. 2007;28(24):3560–3568.
20. Silverman HG, Roberto FF. Understanding marine mussel adhesion. *Mar Biotechnol*. 2007;9(6):661–681.
21. Dove J, Sheridan P. Adhesive protein from mussels: possibilities for dentistry, medicine, and industry. *J Am Dent Assoc*. 1986;112(6):879.
22. Barbara S. Adhesion. *Integr Comp Biol*. 2002;42(6):1172–1180.

23. Hwang DS, Sim SB, Cha HJ. Cell adhesion biomaterial based on mussel adhesive protein fused with RGD peptide. *Biomaterials*. 2007;28(28):4039–4046.

24. Hwang DS, Gim Y, Kang DG, Kim YK, Cha HJ. Recombinant mussel adhesive protein Mgfp-5 as cell adhesion biomaterial. *J Biotechnol*. 2007;127(4):727–735.

25. Lee BP, Messersmith PB, Israelachvili JN, Waite JH. Mussel-inspired adhesives and coatings. *Annu Rev Mater Res*. 2011;41(1):99–132.

26. Lim S, Choi YS, Kang DG, Song YH, Cha HJ. The adhesive properties of coacervated recombinant hybrid mussel adhesive proteins. *Biomaterials*. 2010;31(13):3715–3722.

27. Hwang DS, Zeng H, Srivastava A, et al. Viscosity and interfacial properties in a mussel-inspired adhesive coacervate. *Soft Matter*. 2010;6(14):3232–3236.

28. Madhurakkat Perikamana SK, Lee J, Lee YB, et al. Materials from mussel-inspired chemistry for cell and tissue engineering applications. *Biomacromolecules*. 2015;16(9):2541–2555.

29. Kim HJ, Choi BH, Jun SH, Cha HJ. Sandcastle worm-inspired blood-resistant bone graft binder using a sticky mussel protein for augmented in vivo bone regeneration. *Adv Healthc Mater*. 2016;5(24):3191–3202.

30. Kim BJ, Kim S, Oh DX, Masic A, Cha HJ, Hwang DS. Mussel-inspired adhesive protein-based electrospun nanofibers reinforced by Fe(iii)-DOPA complexation. *J Mater Chem B*. 2015;3(1):112–118.

31. Kim BJ, Oh DX, Kim S, et al. Mussel-mimetic protein-based adhesive hydrogel. *Biomacromolecules*. 2014;15(5):1579–1585.

32. Kim BJ, Cheong H, Hwang BH, Cha HJ. Mussel-inspired protein nanoparticles containing iron(III)-DOPA complexes for pH-responsive drug delivery. *Angew Chemie Int Ed*. 2015;54(25):7318–7322.

33. Choi BH, Cheong H, Jo YK, Bahn SY, Seo JH, Cha HJ. Highly purified mussel adhesive protein to secure biosafety for in vivo applications. *Microb Cell Fact*. 2014;13(1):1–12.

34. Waite JH. Mussel adhesion – essential footwork. *J Exp Biol*. 2017;220(4):517–530.

35. Wang Z, Qin H, Feng Z, et al. Mussel adhesive protein/platelet-rich plasma composite-coated titanium surfaces increase functionality of dermal fibroblasts. *Biotechnol Bioprocess Eng*. 2015;20(3):532–542.

36. Hong JM, Kim BJ, Shim JH, et al. Enhancement of bone regeneration through facile surface functionalization of solid freeform fabrication-based three-dimensional scaffolds using mussel adhesive proteins. *Acta Biomater*. 2012;8(7):2578–2586.

37. Chen L, Komasa S, Hashimoto Y, Hontsu S, Okazaki J. In vitro and in vivo osteogenic activity of titanium implants coated by pulsed laser deposition with a thin film of fluoridated hydroxyapatite. *Int J Mol Sci*. 2018;19:4.

38. Su Y, Komasa S, Li P, et al. Synergistic effect of nanotopography and bioactive ions on peri-implant bone response. *Int J Nanomed*. 2017;12:925–934.

39. Kweon H, Lee SW, Hahn BD, Lee YC, Kim SG. Hydroxyapatite and silk combination-coated dental implants result in superior bone formation in the peri-implant area compared with hydroxyapatite and collagen combination-coated implants. *J Oral Maxillofac Surg*. 2014;72(10):1928–1936.

40. Baty AM, Suci PA, Tyler BJ, Geesey GG. Investigation of mussel adhesive protein adsorption on polystyrene and poly(octadecyl methacrylate) using angle dependent XPS, ATR-FTIR, and AFM. *J Colloid Interface Sci*. 1996;177(2):307–315.

41. Kasuga T, Hiramatsu M, Hoson A, Sekino T, Niihara K. Titania nanotubes prepared by. chemical processing. *Adv Mater*. 1999;11(15):1307–1311.

42. Lee H, Dellatore SM, Miller WM, Messersmith PB. Mussel-inspired surface chemistry for multifunctional coatings. *Science*. 2007;318(5849):426–430.

43. Keselowsky BG, Collard DM, García AJ. Surface chemistry modulates fibronectin conformation and directs integrin binding and specificity to control cell adhesion. *J Biomed Mater Res Part A*. 2003;66A:(2):247–259.

44. Yang K, Lee JS, Kim J, et al. Polydopamine-mediated surface modification of scaffold materials for human neural stem cell engineering. *Biomaterials*. 2012;33(29):6952–6964.

45. Poh CK, Shi Z, Lim TY, Neoh KG, Wang W. The effect of VEGF functionalization of titanium on endothelial cells in vitro. *Biomaterials*. 2010;31(7):1578–1585.

46. Chang KC, Wang Z, Chen S, et al. Dopaminergic enhancement of cellular adhesion in bone marrow derived mesenchymal stem cells (MSCs). *J Stem Cell Res Ther*. 2017;7(8):395.

47. Benhabbour SR, Sheardown H, Adronov A. Cell adhesion and proliferation on hydrophilic dendritically modified surfaces. *Biomaterials*. 2008;29(31):4177–4186.

48. Hopper AP, Dugan JM, Gill AA, et al. Amine functionalized nano-diamond promotes cellular adhesion, proliferation and neurite outgrowth. *Biomed Mater*. 2014;9(4):045009.

49. Arima Y, Iwata H. Effect of wettability and surface functional groups on protein adsorption and cell adhesion using well-defined mixed self-assembled monolayers. *Biomaterials*. 2007;28(20):3074–3082.

50. Desai HV, Voruganti IS, Jayasuriya C, Chen Q, Darling EM. Live-cell, temporal gene expression analysis of osteogenic differentiation in adipose-derived stem cells. *Tissue Eng Part A*. 2013;20(5–6):899–907.

51. Yamaguchi A, Katagiri T, Ikeda T, et al. Recombinant human bone morphogenetic protein-2 stimulates osteoblastic maturation and inhibits myogenic differentiation in vitro. *J Cell Biol*. 1991;113(3):681–687.

52. Cho HJ, Madhurakkat Perikamana SK, Lee JH, et al. Effective immobilization of BMP-2 mediated by polydopamine coating on biodegradable nanofibers for enhanced in vivo bone formation. *ACS Appl Mater Interfaces*. 2014;6(14):11225–11235.

53. Cai Y, Wang X, Khoon C, et al. Colloids and Surfaces B: biointerfaces accelerated bone growth in vitro by the conjugation of BMP2 peptide with hydroxyapatite on titanium alloy. *Colloids Surf B*. 2014;116:681–686.

54. Jun Y, Lee J, Cho H, Keun H, Rim T, Shin H. Electrospun fibers immobilized with bone forming peptide-1 derived from BMP7 for guided bone regeneration. *Biomaterials*. 2013;34(21):5059–5069.

55. Gyune N, Joo S, Min Y, et al. Mussel-inspired surface modification of poly (l -lactide) electrospun fibers for modulation of osteogenic differentiation of human mesenchymal stem cells. *Colloids Surf B*. 2012;91:189–197.

56. Deligianni DD. MWCNTs enhance hBMSCs spreading but delay their proliferation in the direction of differentiation acceleration. *Cell Adhes Migr*. 2014;8(5):487–492.

57. Teo BKK, Wong ST, Lim CK, et al. Nanotopography modulates mechanotransduction of stem cells and induces differentiation through focal adhesion kinase. *ACS Nano*. 2013;7(6):4785–4798.